ACS Photonics

Article

Cite This: ACS Photonics XXXX, XXX, XXX−XXX

pubs.acs.org/journal/apchd5

Room-Temperature Valley Polarization and Coherence in Transition Metal Dichalcogenide−Graphene van der Waals Heterostructures

Etienne Lorchat,[†,§] Stefano Azzini,[‡,§] Thibault Chervy,[‡,§] Takashi Taniguchi,[¶] Kenji Watanabe,[¶] Thomas W. Ebbesen,[‡] Cyriaque Genet,[‡] and Stéphane Berciaud*[,†]

[†]Université de Strasbourg, CNRS, IPCMS, UMR 7504, F-67000 Strasbourg, France

[‡]ISIS & icFRC, Université de Strasbourg and CNRS, UMR 7006, F-67000 Strasbourg, France

[¶]National Institute for Materials Science, Tsukuba, Ibaraki 305-0044, Japan

Supporting Information

ABSTRACT: van der Waals heterostructures made of graphene and transition metal dichalcogenides (TMDs) are an emerging platform for optoelectronic, -spintronic, and -valleytronic devices that could benefit from (i) strong light−matter interactions and spin−valley locking in TMDs and (ii) exceptional electron and spin transport in graphene. The operation of such devices requires significant valley polarization and valley coherence, ideally up to room temperature. Here, using a comprehensive Mueller polarimetry analysis, we report *artifact-free* room-temperature degrees of valley polarization up to 40% and, remarkably, of valley coherence up to 20% in monolayer tungsten disulfide (WS_2)/graphene heterostructures. At a temperature of 20 K, we measure a record degree of valley coherence of 60%, a value that exceeds the degree of valley polarization (50%) and indicates that our samples are minimally affected by pure dephasing processes. Valley contrasts have been particularly elusive in molybdenum diselenide ($MoSe_2$), even at cryogenic temperatures. Upon interfacing monolayer $MoSe_2$ with graphene, the room-temperature degrees of valley polarization and coherence are as high as 14% and 20%, respectively. Our results are discussed in light of recent reports of highly efficient interlayer exciton and carrier transfer in TMD/graphene heterostructures and hold promise for room-temperature chiral light−matter interactions and opto-valleytronic devices.

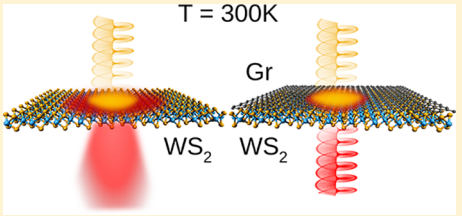

KEYWORDS: *transition metal dichalcogenides, graphene, excitons, spin−valley locking, opto-valleytronics, chiral optics, Mueller polarimetry*

Semiconducting transition metal dichalcogenides (TMDs, with formula MX_2, where M = Mo, W and X = S, Se, Te) are layered materials endowed with exceptional physical properties, which are promising for two-dimensional optoelectronic and opto-valleytronic devices.[1,2] In particular, monolayer TMDs (1L-TMDs) exhibit direct optical bandgaps and exciton binding energies around 20 times larger than the room-temperature thermal energy.[3] Due to the combination of strong spin−orbit coupling and inversion symmetry breaking, 1L-TMDs inherit spin−valley locked properties and chiral optical selection rules.[4] As a result, valley-polarized excitons[5−8] and their coherent superpositions[9] can be formed using circularly and linearly polarized light, respectively, and further manipulated using external fields.[10−13]

Unfortunately, in pristine 1L-TMDs, valley depolarization and valley decoherence occur on picosecond[14−17] and sub-picosecond[10−13] time scales, respectively. As a result, robust valley-contrasting properties have chiefly been demonstrated at cryogenic temperatures,[2,5−9,14,15] where the exciton lifetime is on the order of a few picoseconds only[18] and where phonon-induced intervalley scattering and pure dephasing are minimally efficient. A major challenge is therefore to preserve valley-contrasting properties up to room temperature (RT), where the *effective* exciton lifetime typically exceeds 100 ps in bare 1L-TMDs.[3,18]

Room-temperature valley polarization has been observed in bare 1L-MoS_2[8] or WS_2,[19,20] at the cost of a defect-induced reduction of the excitonic lifetime or, recently, in more complex assemblies, by strongly coupling 1L-WS_2 or 1L-MoS_2 excitons to an optical mode.[21−24] In this case, a cavity protection effect has been invoked to account for RT valley polarization. Noteworthy, valley coherence is directly sensitive to extrinsic and intrinsic pure dephasing mechanisms and hence much more fragile than valley polarization.[13] The largest degrees of valley coherence reported to date reach up to 55% at 4 K in 1L-MoS_2 encapsulated in hexagonal boron nitride (BN).[25] However, RT valley coherence has so far eluded experimental observation until our recent report of a steady state degree of valley coherence of 5% to 8% in WS_2 coupled to a plasmonic array.[21] Overall, obtaining robust RT valley contrasts in high-quality 1L-TMDs is challenging but is, at the same time, a key prerequisite for emerging opto-spintronic and -valleytronic devices.[26,27] Such devices typically interface (i)

Received: September 14, 2018
Published: November 21, 2018

DOI: 10.1021/acsphotonics.8b01306
ACS Photonics XXXX, XXX, XXX−XXX

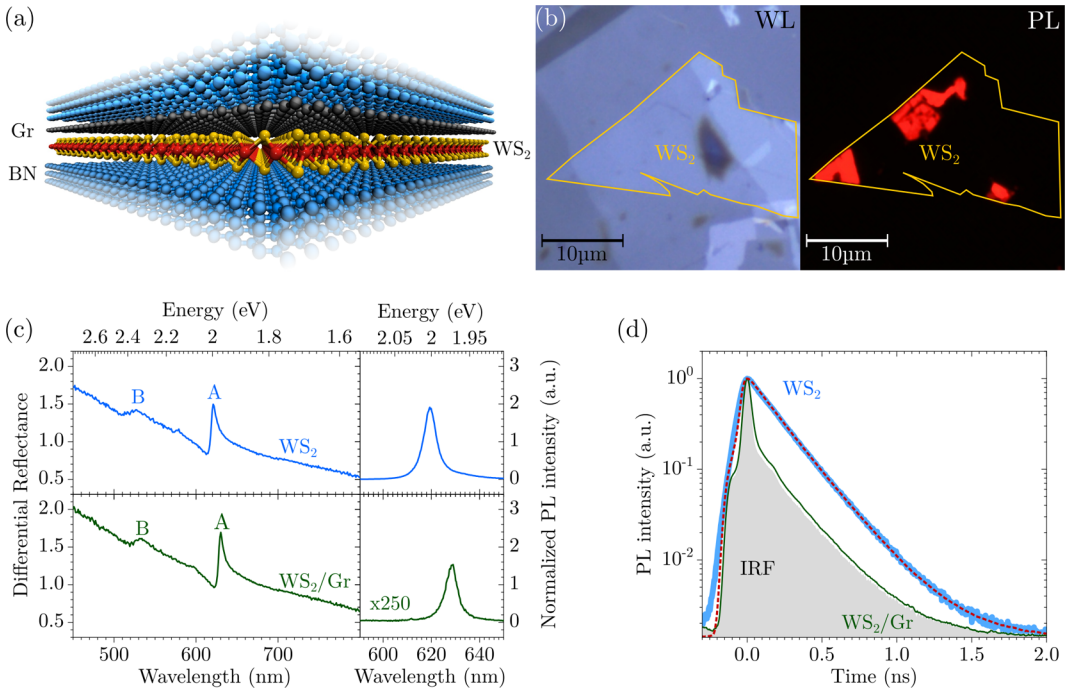

Figure 1. (a) Schematic of a BN-capped 1L-WS_2/Gr heterostructure. (b) White light (WL) and photoluminescence (PL) image of a BN-capped 1L-WS_2/Gr sample. Dark yellow lines highlight the WS_2 monolayer. (c) Differential reflectance (DR) and PL spectra of BN-capped 1L-WS_2 (blue) and BN-capped 1L-WS_2/Gr (green). The PL spectra were recorded in the linear regime, under continuous wave (cw) laser illumination at 532 nm (2.33 eV). (d) PL decay of BN-capped 1L-WS_2 (blue solid line) and BN-capped 1L-WS_2/Gr (green solid line) recorded under pulsed excitation (50 ps pulse duration) at 480 nm (2.58 eV). The instrument response function (IRF) is represented by the gray area. The red dashed line is a monoexponential fit to the BN-capped WS_2 PL decay, yielding an exciton lifetime of 120 ps.

1L-TMDs as a chiral optical material and/or as an injector of spin/valley-polarized electrons with (ii) graphene (Gr), as a high-mobility channel for efficient spin-polarized electron transport.[28−30] In view of their obvious relevance for opto-valleytronics, valley polarization[31] and, crucially, valley coherence in 1L-TMD/Gr heterostructures deserve dedicated investigations.

In this article, we investigate the valley-contrasting properties of van der Waals heterostructures made of 1L-TMD and graphene. In these systems, highly efficient interlayer coupling leads to drastically shortened ($\lesssim$1 ps) 1L-TMD exciton lifetime[32,33] at RT. Valley-polarized excitons can thus quickly recombine radiatively or be directly transferred to graphene before undergoing intervalley scattering and dephasing processes. Using a comprehensive polarimetry analysis based on the Mueller formalism, we uncover RT degrees of valley polarization up to 40% and, remarkably, RT degrees of valley coherence up to 20% in high-quality 1L-WS_2/Gr heterostructures. At a temperature of 20 K, we measure a record degree of valley coherence of 60%, a value that exceeds the degree of valley polarization (50%) and indicates that our samples are minimally affected by pure dephasing processes. Valley contrasts have been particularly elusive in $MoSe_2$, even at cryogenic temperatures.[34] Upon interfacing 1L-$MoSe_2$ with graphene, we observe sizable RT valley polarization of up to 14% and valley coherence as high as 20%. Robust RT valley coherence illustrates the high quality and homogeneity of our samples and opens many perspectives for opto-valleytronic devices that take full benefit from the strong light−matter interactions and spin-valley locked properties of TMDs in combination with exceptional electron and spin transport in graphene.

RESULTS

1L-TMD/Gr heterostructures were fabricated from bulk WS_2, $MoSe_2$, and graphite crystals using a hot pick-up and transfer method introduced by Zomer et al.[35] In order to get rid of environmental- and substrate-induced perturbations, our 1L-TMD/Gr samples were encapsulated using thin BN layers.[25,36] The BN/WS_2/Gr/BN and the BN/$MoSe_2$/Gr/BN stacks were deposited onto transparent glass substrates so that polarization-resolved photoluminescence (PL) measurements could be performed in a transmission configuration. Unless otherwise noted (see Figure 3 for low-temperature data), all measurements described below were performed in ambient air. Samples were systematically excited under sufficiently weak incoming photon flux such that exciton−exciton annihilation[37] could be neglected.

Figure 1 shows (a) the structure and (b) an optical micrograph and a wide-field PL image (obtained using a UV lamp) of the WS_2-based sample. Differential reflectance (DR) spectra (recorded using a white light bulb), PL spectra, and PL decays are reported in Figure 1c and d, respectively. The PL feature arises chiefly from lowest-lying (A) exciton recombination with a faint red-shifted shoulder from charged excitons (trions) (see Figure 2e,i). Due to enhanced dielectric screening from graphene, the PL from BN-capped WS_2/Gr (A exciton at 1.98 eV) is slightly red-shifted as compared to BN-capped WS_2 (A exciton at 2.00 eV).[33,38] As previously reported, non-radiative excitonic energy transfer from WS_2 to graphene, with possible additional contributions due to charge transfer phenomena, lead to massive PL quenching (here, by a factor of ~250) and reduced exciton lifetime,[32,33,39] well below the temporal resolution of our setup (~50 ps). From the ~120 ps RT exciton lifetime in BN-capped WS_2, we may estimate a RT

DOI: 10.1021/acsphotonics.8b01306
ACS Photonics XXXX, XXX, XXX−XXX

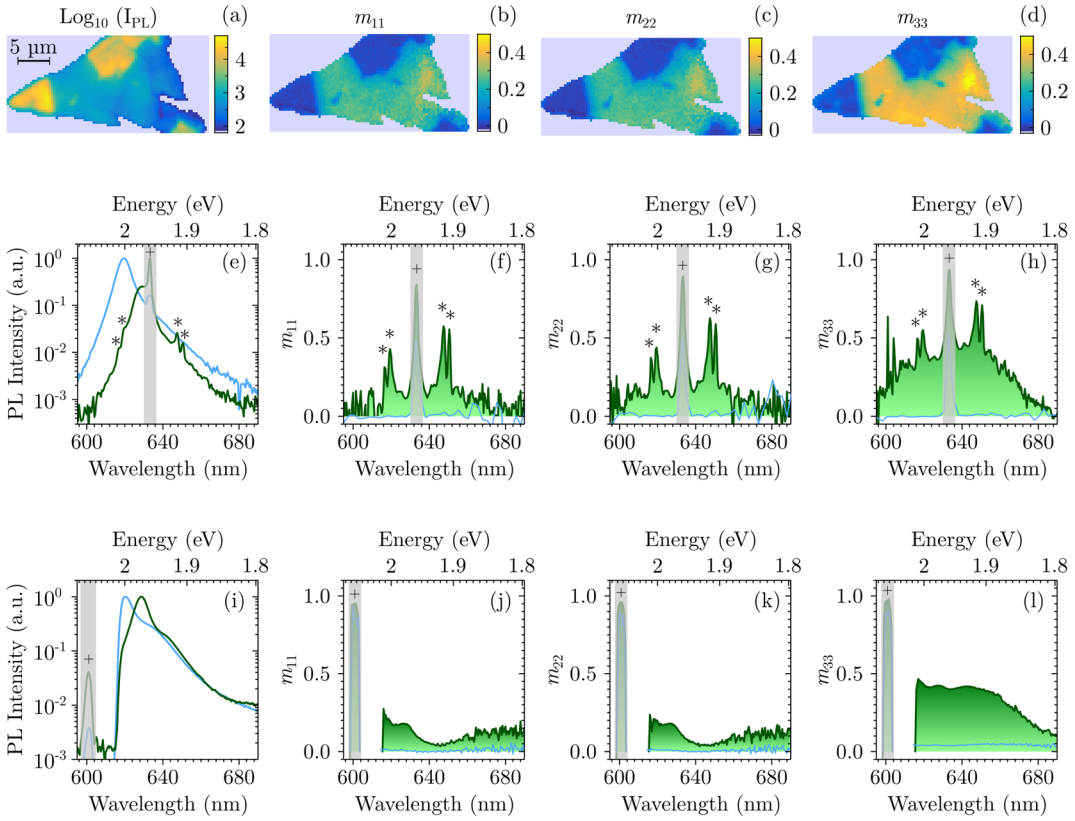

Figure 2. Spatially resolved PL (a) intensity and (b–d) diagonal terms of the Mueller matrix (m_{ii}, i = 1, 2, 3) of the BN-capped WS_2/Gr sample shown in Figure 1 under optical excitation at 1.96 eV. PL spectra (e) and spectrally resolved (f–h) diagonal terms of the Mueller matrix, under optical excitation at 1.96 eV (e(h) and 2.07 eV (i–l). The green (blue) curves correspond to BN-capped WS_2/Gr (BN-capped WS_2). Ultranarrow notch filters with a rejection bandwidth below 1 meV (Optigrate) were used for measurements at 1.96 eV (see (e)–(h)) in order to record the full resonant PL spectrum. The + and * symbols in (e)–(h) highlight residual contributions from the laser beam at the rejection bandwidth of our notch filters and polarization contrasts from WS_2 Raman scattering features, respectively. Note that in (j) and (k) the slight increase of $m_{11,22}$ on the low-energy wing of the WS_2 PL spectrum arises from the faint polarized Raman background from graphene.

exciton lifetime as short as ∼500 fs in BN-capped WS_2/Gr. Similar measurements in BN-capped $MoSe_2$/Gr are reported in the Supporting Information, Figure S10. Even if our experimental apparatus does not make it possible to resolve the exciton lifetime in TMD/Gr, the values we estimate here are fully consistent with recent photoluminescence and transient absorption spectroscopy, which consistently reported room-temperature exciton lifetimes of 1 ps or slightly less in TMD/Gr.[32,33,39]

To date, valley polarization in TMDs has been assessed through measurements of the degree of circular polarization, $\rho^{\pm} = \frac{I_{\sigma_\pm}(\sigma^+) - I_{\sigma_\pm}(\sigma^-)}{I_{\sigma_\pm}(\sigma^+) + I_{\sigma_\pm}(\sigma^-)}$, where $I_j(l)$ is the measured PL spectrum for a $j = (\sigma^+,\sigma^-)$ polarized excitation and a $l = (\sigma^+,\sigma^-)$ polarized analysis. Similarly, the degree of valley coherence has been considered equal to the degree of linear polarization, $\gamma = \frac{I_{\parallel} - I_{\perp}}{I_{\parallel} + I_{\perp}}$, measured under linearly polarized excitation with an arbitrary orientation with respect to the TMD crystal lattice and where $I_{\parallel}$ (respectively $I_{\perp}$) denote the PL intensity for parallel (respectively perpendicular) linear polarizations of the incoming and emitted photons. As explained in the Supporting Information (Section S2), this correspondence is only valid in the absence of any contribution from (i) circular or linear dichroism and (ii) polarization-dependent PL quantum yield. Owing to their highly symmetric hexagonal crystal structure (D_{3h} point group), 1L-TMDs feature isotropic absorption and emission following optical excitation polarized in the layer plane.[3,4] However, symmetry breaking may arise when TMD monolayers are deposited on substrates and perhaps even more critically when they are interfaced with other 2D materials such as graphene. Besides, it is known that well-defined polarization states are challenging to maintain in optical microscopy setups, mostly due to focusing optics and polarization-sensitive beamsplitters. These symmetry-related and instrumental aspects are prone to lead to artifacts when it comes to quantitatively measuring the degree of circular and linear polarizations and hence assessing the valley contrasts.

In order to provide an *artifact-free* measurement of the valley contrasts, we make use of a home-built polarimetry setup that allows us to measure the 4 × 4 Mueller matrix $\mathcal{M}$ associated with the spatially and spectrally resolved PL response of our samples. The Mueller matrix connects arbitrary incoming polarization states (defined by the Stokes vector $\mathbf{S}^{in}$ of the pump laser beam) to the outgoing Stokes vector $\mathbf{S}^{out}$ associated with the light emitted by the sample such that[40−42]

$$\mathbf{S}^{out} = \mathcal{M}\cdot\mathbf{S}^{in}, \text{ with } \mathbf{S}^{out,\,in} = \begin{pmatrix} I_0 \\ I_V - I_H \\ I_{45} - I_{-45} \\ I_{\sigma^+} - I_{\sigma^-} \end{pmatrix}_{out,\,in} \quad (1)$$

DOI: 10.1021/acsphotonics.8b01306
ACS Photonics XXXX, XXX, XXX−XXX

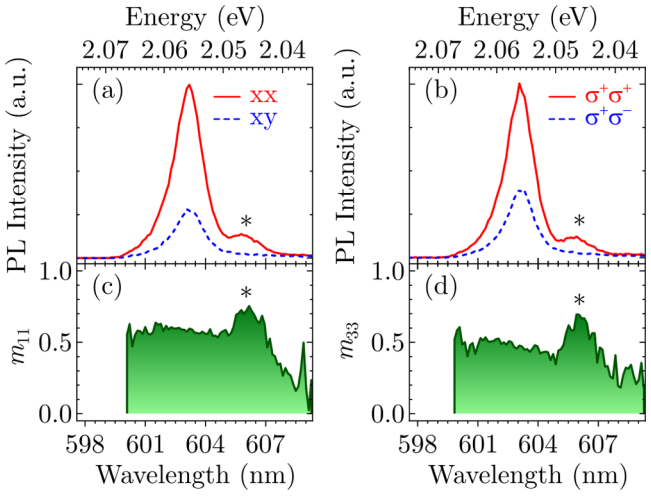

Figure 3. (a, b) Low-temperature polarization-resolved photoluminescence spectra of the bright exciton line of the BN-capped WS_2/Gr sample shown in Figure 2. The sample is held at a temperature of 20 K and excited near resonance at 590 nm (2.10 eV) by linearly (x) and circularly (σ^+) polarized photons in (a) and (b), respectively. Polarization-resolved spectra in co- and cross-linear configurations (in (a), xx and xy in red and blue, respectively) as well as co- and cross-circular configurations (in (b), $\sigma^+\sigma^+$ and $\sigma^+\sigma^-$ in red and blue, respectively) are shown. The associated degrees of valley coherence (m_{11}) and valley polarization (m_{33}) are shown in (c) and (d), respectively. The * symbols highlight contributions from WS_2 Raman scattering features, as in Figure 2.

where I_0 is the emitted (incident) intensity, I_V-I_H is the relative intensity in vertical and horizontal polarizations, $I_{45}-I_{-45}$ is the relative intensity in +45° and −45° linear polarizations, $I_{\sigma^+}-I_{\sigma^-}$ is the relative intensity in σ^+ and σ^- circular polarizations, and the "in" ("out") labels the incident (emitted) state of light. More details on our Mueller polarimetry setup can be found in the Supporting Information, Section S2 and Figure S1.

In the present study, the most relevant elements of the Mueller matrix $\mathcal{M}$ are its diagonal terms m_{ii}, with i = 0, 1, 2, 3. By definition, m_{00} corresponds to the PL intensity and is normalized to unity at all measured wavelengths. Hence, the PL spectra shown in Figure 2a,e and Figure 4a,e in arbitrary units correspond to m_{00} recorded under unpolarized excitation, without any polarization analysis and prior normalization. With this definition of m_{00}, the degrees of valley polarization and valley coherence are rigorously equal to m_{33} and m_{11} (or m_{22}), respectively. Circular and linear dichroism correspond to m_{03} and m_{01}, m_{02}, respectively, whereas polarization-dependent PL quantum yields are accounted for by m_{i0}, i = 1, 2, 3. In the Mueller formalism, i = 1 (respectively i = 2) refers to vertical/horizontal (respectively ±45°) linear polarizations relative to an arbitrary reference angle. Based on symmetry properties, $\mathcal{M}$ is expected to be diagonal in bare 1L-TMDs, with $m_{11} = m_{22}$. As we verify experimentally, the off-diagonal elements of the Mueller matrix are indeed negligible (see Supporting Information, Figures S2−S4 and S7). This *sanity check* is of utmost importance, as it justifies *a posteriori* that the simple and widespread measurements of the degrees of circular and linear polarization[2,3,5−9] are usually sufficient to get a reliable estimation of the degrees of valley polarization and coherence. Nevertheless, let us stress that only a comprehensive Mueller polarimetry analysis is able to unambiguously quantify valley-contrasting properties (see Supporting Information, Sec. S2.3).

Figure 2 displays the spatially and spectrally resolved diagonal elements of the Mueller matrix of the sample shown in Figure 1. The maps in Figure 2a−d correspond to spectrally integrated PL intensity (Figure 2a), valley coherence ($m_{11,22}$, Figure 2b,c), and valley polarization m_{33} upon laser excitation at 1.96 eV. A clear anticorrelation between the total PL intensity and the valley contrasts appears, with near-zero valley contrasts in BN-capped WS_2 (bright regions in Figures 1b and 2a) and large degrees of valley polarization and coherence in BN-capped WS_2/Gr. To quantitatively assess the valley contrasts, we resort to spectrally resolved measurements at two different laser excitation energies, very close to (1.96 eV, i.e., 633 nm; see Figure 2e−h) or slightly above (2.07 eV, i.e., 600 nm, see Figure 2i−l) the optical bandgap of BN-capped WS_2/Gr. In stark contrast with the total absence of valley contrasts in our BN-capped WS_2 sample ($m_{ii,i=1,2,3} \approx 0$), BN-capped WS_2/Gr exhibits large valley polarization ($m_{33} \approx 40\%$) *and* coherence ($m_{11} \approx m_{22} \approx 20\%$) over the entire span of the PL spectrum. In Figure 2f−h, these contrasts give rise to a baseline on which five sharp peaks with larger contrasts emerge. These peaks correspond to a faint laser residue and to polarization-sensitive Stokes and anti-Stokes Raman scattering features from (i) the out-of-plane A'_1 phonon (near 1.907 eV on the Stokes side) and (ii) the resonant 2LA(M) mode (near 1.915 eV on the Stokes side).[43] Note that the in-plane E' feature is expected to overlap with the 2LA(M) feature but has a vanishingly small intensity under laser excitation at 1.96 eV. The proposed assignments are unambiguously confirmed by high-resolution polarized Raman measurements (see Supporting Information, Figure S9). Very similar results are observed (Figure 2i−l) when exciting the sample at 2.07 eV, except for the fact that no spurious contributions from Raman features are observed. Similar valley contrasts were observed in another BN-capped WS_2/Gr sample and in SiO_2-supported WS_2/Gr samples either exposed to ambient air (not shown) or covered by a LiF epilayer (see Supporting Information, Figure S5).

To better gauge these large RT valley contrasts, we now compare the results in Figure 2 with the valley contrasts recorded in the same BN-capped WS_2/Gr sample at cryogenic temperature. As shown in Figure 3, the bright neutral exciton, measured at 2.056 eV (with a narrow full width at half-maximum of 5 meV), exhibits high values of $m_{33} \approx 50\%$ and $m_{11} \approx 60\%$ at 20 K. This degree of valley coherence is 3 times larger than at RT and is to our knowledge the highest value reported so far in a 1L-TMD-based system. Conversely, excitons in BN-capped WS_2 only exhibit modest valley polarization ($m_{33} \approx 10\%$) and coherence ($m_{11} \approx 15\%$) at similar temperatures (see Supporting Information, Figure S6).

To further evidence that graphene enables improved valley contrasts, we finally consider the RT Mueller matrix of $MoSe_2$/Gr. Indeed, robust valley polarization remains elusive in bare $MoSe_2$, even at low temperature.[34,44] The microscopic mechanisms responsible for accelerated valley depolarization and decoherence in $MoSe_2$ remain a topic of ongoing research.[3,34] Figure 4 shows the RT PL spectra and $m_{ii,i=1-3}$ in BN-capped $MoSe_2$/Gr compared to a reference in a BN-capped $MoSe_2$ sample, wherein a short excitonic lifetime (and thus potentially measurable valley contrasts) was observed (see Supporting Information, Figure S10). The A exciton in BN-capped $MoSe_2$/Gr (respectively BN-capped $MoSe_2$) is found at 1.568 eV (respectively 1.573 eV), and the higher order B

DOI: 10.1021/acsphotonics.8b01306
ACS Photonics XXXX, XXX, XXX−XXX

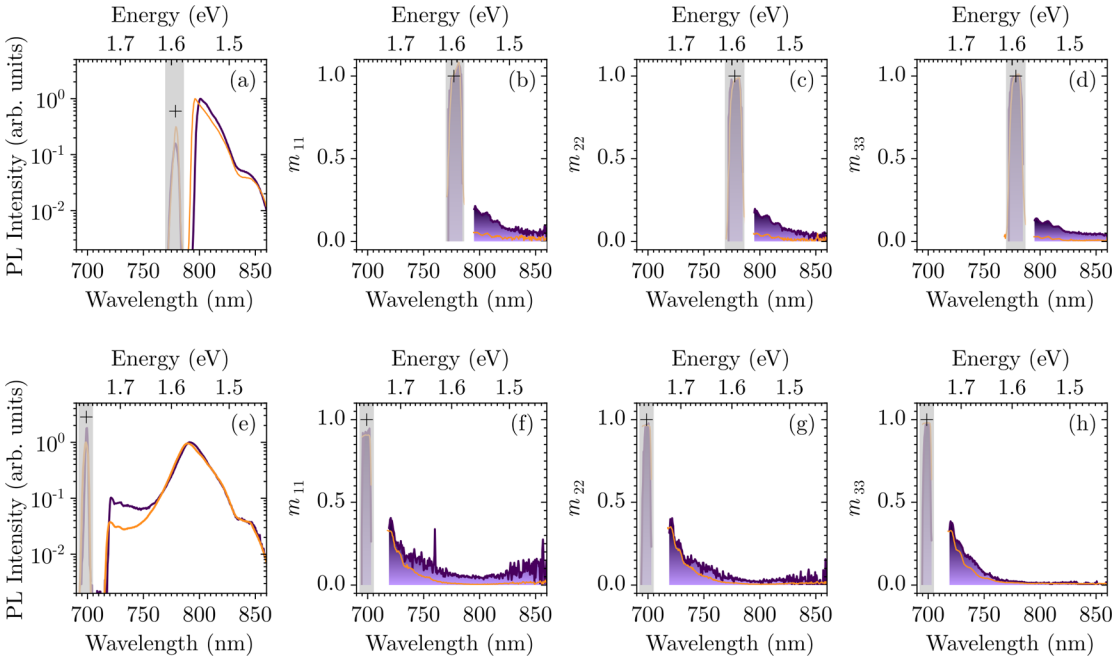

Figure 4. PL spectra and spectrally resolved diagonal terms of the Mueller matrix (m_{ii}, i = 1, 2, 3) of a BN-capped $MoSe_2$/Gr sample under optical excitation at 780 nm (i.e., 1.59 eV) (a–d) and 700 nm (i.e., 1.77 eV) (e–h). The purple (respectively orange) curves correspond to BN-capped $MoSe_2$/Gr (respectively BN-capped $MoSe_2$). The + symbols highlight residual contributions from the laser beam. The locations of the A and B exciton features are indicated.

exciton lies near 1.77 eV. Under quasi resonant excitation at 1.59 eV (i.e., 780 nm; see Figure 4a–d), we measure a degree of valley polarization $m_{33} \approx 14\%$ near the A exciton peak energy in BN-capped $MoSe_2$/Gr. Remarkably, the RT degree of valley coherence $m_{11,22} \approx 20\%$ in BN-capped $MoSe_2$/Gr exceeds m_{33}. Conversely, $m_{11,22} \approx 5\%$ and $m_{33} \approx 2\%$ in BN-capped $MoSe_2$. Under excitation at 1.77 eV (i.e., 700 nm; see Figure 4a–d), slightly above the B exciton, we observe vanishingly small valley contrasts associated with the A exciton. However, "hot" PL from the B exciton exhibits a large degree of valley polarization and coherence, both up to 40% (respectively 35%) in BN-capped $MoSe_2$/Gr (respectively BN-capped $MoSe_2$). Interestingly, similar valley contrasts are also observed under excitation at 1.50 eV (i.e., 825 nm), slightly below the $MoSe_2$ bandgap (see Supporting Information, Figure S8).

DISCUSSION

Our study demonstrates that robust RT valley polarization and coherence can now be generated optically in systems based on 1L-TMD. Importantly, using Mueller polarimetry in 1L-TMD/Gr heterostructures, we experimentally demonstrate that $m_{11} = m_{22}$ and that $m_{ij,j\neq i} \approx 0$ (see Supporting Information, Figures S2–S4 and S7), such that circular dichroism and birefringence can safely be neglected.

At the microscopic level, RT valley contrasts in our TMD/Gr samples are a direct consequence of highly efficient nonradiative exciton decay in 1L-TMD/Gr.[33] The observation of radiative recombination of valley-polarized excitons and of their coherent superpositions is thus restricted to short ($\lesssim$1 ps) time scales that are comparable with typical valley depolarization and decoherence times. In other words, as illustrated in Figure 5, long-lived excitons that would undergo spin scattering and dephasing processes in bare 1L-TMD are efficiently filtered out by the near-field coupled graphene layer. Along this line, valley contrasts associated with B exciton emission in $MoSe_2$ and $MoSe_2$/Gr (see Figure 4f–h) also stem from the sub-picosecond lifetime of these higher-order states.

Assuming full valley polarization under circularly polarized continuous wave (cw) excitation, we can estimate a steady state degree of valley polarization, $m_{33} = \left(1 + 2\frac{\Gamma_S}{\Gamma_X}\right)^{-1}$, where Γ_X denotes the exciton decay rate and Γ_S the exciton spin scattering rate, respectively[5] (see also Figure 5). Assuming $\Gamma_X^{-1} \approx 500$ fs, and considering our measured values of m_{33}, we estimate $\Gamma_S^{-1} \approx 600$ fs in WS_2/Gr and $\Gamma_S^{-1} \approx 150$ fs in $MoSe_2$/Gr. These values are slightly smaller than valley depolarization times measured at intermediate temperatures (near 125 K) in TMD monolayers deposited on SiO_2.[16] It is therefore likely that the presence of graphene (in addition to that of the capping BN thin layers) will not drastically affect valley depolarization. Along this line, it is interesting to notice that m_{33} is nearly the same in WS_2/Gr at ~20 K and 300 K. Such a situation is conceivable since (i) the exciton lifetime in TMD/Gr is quite close to the particularly short lifetime of excitons residing within the light cone of bare 1L-TMD (ranging between a few hundreds of fs and 2 ps[18,45]) and (ii) the exciton spin scattering rate does not show very strong temperature dependence.[16] In any event, care has to be taken when comparing degrees of valley polarization measured in different systems and possibly in different conditions because it is not clear whether absorption of near-resonant circularly polarized photons will lead to full valley polarization, in particular in WS_2, a material with a lower lying dark state.[3]

The fact that the degrees of valley coherence $m_{11,22}$ are approaching (in WS_2/Gr) or even exceeding (in WS_2/Gr at 20 K and in $MoSe_2$/Gr at 300 K) m_{33} indicates that the dominant mechanism that limits valley polarization is almost exclusively responsible for valley decoherence. Indeed, when pure dephasing is negligible, the valley–exciton decoherence time

DOI: 10.1021/acsphotonics.8b01306
ACS Photonics XXXX, XXX, XXX–XXX

is twice the lifetime of the valley−exciton polarization.[46] Such a near-ideal case had so far only been reported in BN-capped MoS_2 at 4 K[25] and is now reachable in ambient conditions using TMD/Gr heterostructures.

At present, exciton spin scattering mediated by the exchange interaction is thought to be the dominant depolarization and decoherence mechanism.[3,9,13,16] Alternate mechanisms based on electron−phonon interactions have also been considered separately.[17] Temperature-dependent Mueller polarimetry in TMD/Gr samples would provide invaluable insights that could be confronted to a full theoretical framework that considers the competition between exchange- and phonon-mediated depolarization. Such studies go outside the scope of our work, which focuses on the robustness of RT valley contrasts.

We note that the RT valley contrasts reported above come at the cost of significant PL quenching and short exciton lifetimes. Nevertheless, the PL intensity in TMD/Gr has recently been shown to scale linearly with the incident photon fluxes up to values in excess of 10^{24} cm^{-2} s^{-1} (i.e., typically a visible laser beam of 1 mW focused onto a diffraction-limited spot[33]). In contrast, under these conditions, the PL efficiency of bare 1L-TMD is massively reduced due to exciton−exciton annihilation effects and lies close to that of 1L-TMD/Gr.[33] More broadly, 1L-TMD/Gr heterostructures feature major advantages as compared to related systems, in which RT valley contrasts have recently been unveiled. First, even in the absence of BN capping layers, 1L-TMD/Gr have been shown to be well-defined systems with smooth interfaces and highly reproducible photophysical properties.[33] RT valley contrasts can thus consistently be observed in minimally defective TMD/Gr samples. This result is in stark contrast with recent reports in bare 1L-TMD, in which RT valley polarizations are observable only when structural defects or extrinsic environmental effects provide sufficiently fast nonradiative exciton decay pathways as compared to depolarization times.[20] The large degrees of valley coherence achieved here are very unlikely to occur in such defective samples. Second, owing to the excellent electron and spin transport properties of Gr, high-quality 1L-TMD/Gr heterostructures can easily be electrically connected and integrated in chiral light-emitting systems[47] and opto-spintronic circuits.[26,27]

CONCLUSION

We have demonstrated that monolayer transition metal dichalcogenides (here, WS_2 and $MoSe_2$) directly stacked onto monolayer graphene provide highly stable room-temperature chiral light emitters, in spite of inevitable photoluminescence quenching. Similar valley-contrasting properties are expected in other TMD/graphene heterostructures using MoS_2, WSe_2, and possibly near-infrared-emitting $MoTe_2$,[48,49] where, as in bare $MoSe_2$, valley contrasts remain elusive.[50] Our complete analysis, based on the Mueller formalism, provides *artifact-free* measurements of valley polarization and valley coherence. As such, it goes beyond state-of-the-art polarimetry in transition metal dichalcogenides, which so far has relied on measurements of circular and linear polarization contrasts.[3,4,9,51] We anticipate further implementations of Mueller polarimetry to investigate chiral light−matter interactions not only in transition metal dichalcogenides (in particular in bilayer or few-layer systems[52−54]) but also in other emerging two-dimensional systems, such as two-dimensional ferromagnets[55] and van der Waals heterostructures based on the latter.[56] Besides direct implementations in novel opto-valleytronic devices, robust generation of room-temperature valley-polarized excitons and, importantly, of valley coherence invites further investigations in nanophotonics, in particular in the chiral strong coupling regime.[21]

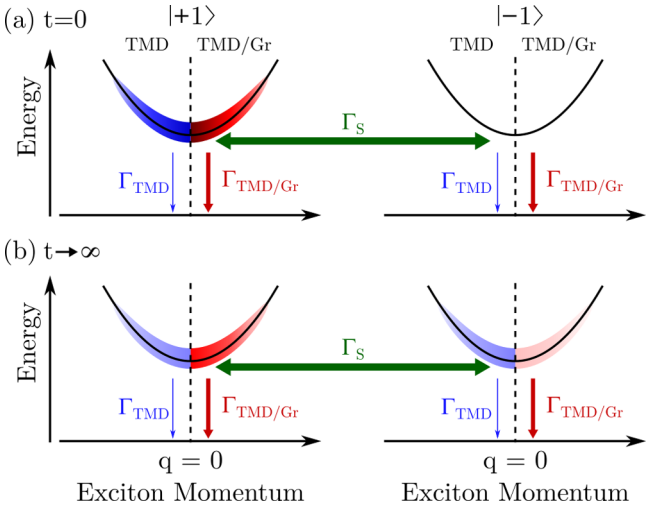

Figure 5. Sketches, in the momentum-energy space, of valley−exciton dynamics in bare 1L-TMD compared to 1L-TMD/Gr. Γ_X, with X = TMD, TMD/Gr, denotes the band-edge exciton decay rate of the bare 1L-TMD and of the 1L-TMD/Gr heterostructure, respectively. Γ_S is the exciton spin scattering rate. Exciton populations with ±1 valley pseudospin are illustrated with blue (TMD) and red (TMD/Gr) contours. Darker shades correspond to larger populations. The top panel (a) depicts full valley polarization following optical pumping using circularly polarized photons. The bottom panel (b) represents the populations of valley excitons in the steady state.

ASSOCIATED CONTENT

Supporting Information

The Supporting Information is available free of charge on the ACS Publications website at DOI: 10.1021/acsphotonics.8b01306.

Additional details on methods; Mueller polarimetry; full Mueller matrices measured on BN-capped WS_2/Gr and BN-capped $MoSe_2$/Gr; helicity-resolved PL spectra on WS_2/graphene; low-temperature polarization-resolved PL on BN-capped WS_2; high-resolution Raman measurements on WS_2/Gr; optical characterization of BN-capped $MoSe_2$/graphene (PDF)

AUTHOR INFORMATION

Corresponding Author

*E-mail: stephane.berciaud@ipcms.unistra.fr.

ORCID

Kenji Watanabe: 0000-0003-3701-8119
Thomas W. Ebbesen: 0000-0002-3999-1636
Cyriaque Genet: 0000-0003-0672-7406
Stéphane Berciaud: 0000-0002-5753-3671

Author Contributions

§E. Lorchat, S. Azzini, and T. Chervy contributed equally to this study.

Notes

The authors declare no competing financial interest.

DOI: 10.1021/acsphotonics.8b01306
ACS Photonics XXXX, XXX, XXX−XXX

■ ACKNOWLEDGMENTS

We thank X. Marie, C. Robert, and D. Lagarde for fruitful discussions; J. Hone and D. Chenet for valuable advice on sample fabrication; and A. Boulard, F. Chevrier, and the STNano clean room staff for technical assistance. This work was supported in part by the ANR Equipex "Union" (ANR-10-EQPX-52-01), ANR Grant (H2DH ANR-15-CE24-0016), the Labex NIE projects (ANR-11-LABX-0058-NIE) and USIAS within the Investissement d'Avenir program ANR-10-IDEX-0002-02. S.B. is a member of the Institut Universitaire de France (IUF).

■ REFERENCES

(1) Mak, K. F.; Shan, J. Photonics and optoelectronics of 2D semiconductor transition metal dichalcogenides. *Nat. Photonics* **2016**, *10*, 216−226.
(2) Schaibley, J. R.; Yu, H.; Clark, G.; Rivera, P.; Ross, J. S.; Seyler, K. L.; Yao, W.; Xu, X. Valleytronics in 2D materials. *Nature Reviews Materials* **2016**, *1*, 16055.
(3) Wang, G.; Chernikov, A.; Glazov, M. M.; Heinz, T. F.; Marie, X.; Amand, T.; Urbaszek, B. Colloquium: Excitons in atomically thin transition metal dichalcogenides. *Rev. Mod. Phys.* **2018**, *90*, 021001.
(4) Xu, X.; Yao, W.; Xiao, D.; Heinz, T. F. Spin and pseudospins in layered transition metal dichalcogenides. *Nat. Phys.* **2014**, *10*, 343−350.
(5) Mak, K. F.; He, K.; Shan, J.; Heinz, T. F. Control of valley polarization in monolayer MoS_2 by optical helicity. *Nat. Nanotechnol.* **2012**, *7*, 494−498.
(6) Zeng, H.; Dai, J.; Yao, W.; Xiao, D.; Cui, X. Valley polarization in MoS2 monolayers by optical pumping. *Nat. Nanotechnol.* **2012**, *7*, 490−493.
(7) Cao, T.; Wang, G.; Han, W.; Ye, H.; Zhu, C.; Shi, J.; Niu, Q.; Tan, P.; Wang, E.; Liu, B.; Feng, J. Valley-selective circular dichroism of monolayer molybdenum disulphide. *Nat. Commun.* **2012**, *3*, 887.
(8) Sallen, G.; Bouet, L.; Marie, X.; Wang, G.; Zhu, C. R.; Han, W. P.; Lu, Y.; Tan, P. H.; Amand, T.; Liu, B. L.; Urbaszek, B. Robust optical emission polarization in MoS_2 monolayers through selective valley excitation. *Phys. Rev. B: Condens. Matter Mater. Phys.* **2012**, *86*, 081301.
(9) Jones, A. M.; Yu, H.; Ghimire, N. J.; Wu, S.; Aivazian, G.; Ross, J. S.; Zhao, B.; Yan, J.; Mandrus, D. G.; Xiao, D.; Yao, W.; Xu, X. Optical generation of excitonic valley coherence in monolayer WSe_2. *Nat. Nanotechnol.* **2013**, *8*, 634−638.
(10) Ye, Z.; Sun, D.; Heinz, T. F. Optical manipulation of valley pseudospin. *Nat. Phys.* **2016**, *13*, 26.
(11) Wang, G.; Marie, X.; Liu, B. L.; Amand, T.; Robert, C.; Cadiz, F.; Renucci, P.; Urbaszek, B. Control of Exciton Valley Coherence in Transition Metal Dichalcogenide Monolayers. *Phys. Rev. Lett.* **2016**, *117*, 187401.
(12) Schmidt, R.; Arora, A.; Plechinger, G.; Nagler, P.; Granados del Águila, A.; Ballottin, M. V.; Christianen, P. C. M.; Michaelis de Vasconcellos, S.; Schüller, C.; Korn, T.; Bratschitsch, R. Magnetic-Field-Induced Rotation of Polarized Light Emission from Monolayer WS_2. *Phys. Rev. Lett.* **2016**, *117*, 077402.
(13) Hao, K.; Moody, G.; Wu, F.; Dass, C. K.; Xu, L.; Chen, C.-H.; Sun, L.; Li, M.-Y.; Li, L.-J.; MacDonald, A. H.; Li, X. Direct measurement of exciton valley coherence in monolayer WSe_2. *Nat. Phys.* **2016**, *12*, 677.
(14) Lagarde, D.; Bouet, L.; Marie, X.; Zhu, C. R.; Liu, B. L.; Amand, T.; Tan, P. H.; Urbaszek, B. Carrier and Polarization Dynamics in Monolayer MoS_2. *Phys. Rev. Lett.* **2014**, *112*, 047401.
(15) Wang, G.; Bouet, L.; Lagarde, D.; Vidal, M.; Balocchi, A.; Amand, T.; Marie, X.; Urbaszek, B. Valley dynamics probed through charged and neutral exciton emission in monolayer WSe_2. *Phys. Rev. B: Condens. Matter Mater. Phys.* **2014**, *90*, 075413.
(16) Zhu, C. R.; Zhang, K.; Glazov, M.; Urbaszek, B.; Amand, T.; Ji, Z. W.; Liu, B. L.; Marie, X. Exciton valley dynamics probed by Kerr rotation in WS_2 monolayers. *Phys. Rev. B: Condens. Matter Mater. Phys.* **2014**, *90*, 161302.
(17) Molina-Sánchez, A.; Sangalli, D.; Wirtz, L.; Marini, A. Ab Initio Calculations of Ultrashort Carrier Dynamics in Two-Dimensional Materials: Valley Depolarization in Single-Layer WSe2. *Nano Lett.* **2017**, *17*, 4549−4555.
(18) Robert, C.; Lagarde, D.; Cadiz, F.; Wang, G.; Lassagne, B.; Amand, T.; Balocchi, A.; Renucci, P.; Tongay, S.; Urbaszek, B.; Marie, X. Exciton radiative lifetime in transition metal dichalcogenide monolayers. *Phys. Rev. B: Condens. Matter Mater. Phys.* **2016**, *93*, 205423.
(19) Nayak, P. K.; Lin, F.-C.; Yeh, C.-H.; Huang, J.-S.; Chiu, P.-W. Robust room temperature valley polarization in monolayer and bilayer WS2. *Nanoscale* **2016**, *8*, 6035−6042.
(20) McCreary, K. M.; Currie, M.; Hanbicki, A. T.; Chuang, H.-J.; Jonker, B. T. Understanding Variations in Circularly Polarized Photoluminescence in Monolayer Transition Metal Dichalcogenides. *ACS Nano* **2017**, *11*, 7988−7994.
(21) Chervy, T.; Azzini, S.; Lorchat, E.; Wang, S.; Gorodetski, Y.; Hutchison, J. A.; Berciaud, S.; Ebbesen, T. W.; Genet, C. Room Temperature Chiral Coupling of Valley Excitons with Spin-Momentum Locked Surface Plasmons. *ACS Photonics* **2018**, *5*, 1281.
(22) Chen, Y.-J.; Cain, J. D.; Stanev, T. K.; Dravid, V. P.; Stern, N. P. Valley-polarized exciton-polaritons in a monolayer semiconductor. *Nat. Photonics* **2017**, *11*, 431.
(23) Sun, Z.; Gu, J.; Ghazaryan, A.; Shotan, Z.; Considine, C. R.; Dollar, M.; Chakraborty, B.; Liu, X.; Ghaemi, P.; Kéna-Cohen, S.; Menon, V. M. Optical control of room-temperature valley polaritons. *Nat. Photonics* **2017**, *11*, 491.
(24) Lundt, N.; Stoll, S.; Nagler, P.; Nalitov, A.; Klembt, S.; Betzold, S.; Goddard, J.; Frieling, E.; Kavokin, A. V.; Schüller, C.; Korn, T.; Höfling, S.; Schneider, C. Observation of macroscopic valley-polarized monolayer exciton-polaritons at room temperature. *Phys. Rev. B: Condens. Matter Mater. Phys.* **2017**, *96*, 241403.
(25) Cadiz, F.; Courtade, E.; Robert, C.; Wang, G.; Shen, Y.; Cai, H.; Taniguchi, T.; Watanabe, K.; Carrere, H.; Lagarde, D.; Manca, M.; Amand, T.; Renucci, P.; Tongay, S.; Marie, X.; Urbaszek, B. Excitonic Linewidth Approaching the Homogeneous Limit in MoS_2-Based van der Waals Heterostructures. *Phys. Rev. X* **2017**, *7*, 021026.
(26) Luo, Y. K.; Xu, J.; Zhu, T.; Wu, G.; McCormick, E. J.; Zhan, W.; Neupane, M. R.; Kawakami, R. K. Opto-Valleytronic Spin Injection in Monolayer MoS_2/Few-Layer Graphene Hybrid Spin Valves. *Nano Lett.* **2017**, *17*, 3877−3883.
(27) Avsar, A.; Unuchek, D.; Liu, J.; Sanchez, O. L.; Watanabe, K.; Taniguchi, T.; zyilmaz, B.; Kis, A. Optospintronics in Graphene via Proximity Coupling. *ACS Nano* **2017**, *11*.11678
(28) Han, W.; Kawakami, R. K.; Gmitra, M.; Fabian, J. Graphene spintronics. *Nat. Nanotechnol.* **2014**, *9*, 794.
(29) Ghiasi, T. S.; Ingla-Ayns, J.; Kaverzin, A. A.; van Wees, B. J. Large Proximity-Induced Spin Lifetime Anisotropy in Transition-Metal Dichalcogenide/Graphene Heterostructures. *Nano Lett.* **2017**, *17*, 7528−7532.
(30) Benítez, L. A.; Sierra, J. F.; Savero Torres, W.; Arrighi, A.; Bonell, F.; Costache, M. V.; Valenzuela, S. O. Strongly anisotropic spin relaxation in graphene-transition metal dichalcogenide heterostructures at room temperature. *Nat. Phys.* **2018**, *14*, 303.
(31) Du, L.; Zhang, Q.; Gong, B.; Liao, M.; Zhu, J.; Yu, H.; He, R.; Liu, K.; Yang, R.; Shi, D.; Gu, L.; Yan, F.; Zhang, G.; Zhang, Q. Robust spin-valley polarization in commensurate MoS_2/graphene heterostructures. *Phys. Rev. B: Condens. Matter Mater. Phys.* **2018**, *97*, 115445.
(32) He, J.; Kumar, N.; Bellus, M. Z.; Chiu, H.-Y.; He, D.; Wang, Y.; Zhao, H. Electron transfer and coupling in graphene−tungsten disulfide van der Waals heterostructures. *Nat. Commun.* **2014**, *5*, 5622.
(33) Froehlicher, G.; Lorchat, E.; Berciaud, S. Charge Versus Energy Transfer in Atomically Thin Graphene-Transition Metal Dichalcogenide van der Waals Heterostructures. *Phys. Rev. X* **2018**, *8*, 011007.

DOI: 10.1021/acsphotonics.8b01306
ACS Photonics XXXX, XXX, XXX−XXX

(34) Wang, G.; Palleau, E.; Amand, T.; Tongay, S.; Marie, X.; Urbaszek, B. Polarization and time-resolved photoluminescence spectroscopy of excitons in $MoSe_2$ monolayers. *Appl. Phys. Lett.* **2015**, *106*, 112101.
(35) Zomer, P. J.; Guimarães, M. H. D.; Brant, J. C.; Tombros, N.; van Wees, B. J. Fast pick up technique for high quality heterostructures of bilayer graphene and hexagonal boron nitride. *Appl. Phys. Lett.* **2014**, *105*, 013101.
(36) Ajayi, O. A.; Ardelean, J. V.; Shepard, G. D.; Wang, J.; Antony, A.; Taniguchi, T.; Watanabe, K.; Heinz, T. F.; Strauf, S.; Zhu, X.-Y.; Hone, J. C. Approaching the intrinsic photoluminescence linewidth in transition metal dichalcogenide monolayers. *2D Mater.* **2017**, *4*, 031011.
(37) Kumar, N.; Cui, Q.; Ceballos, F.; He, D.; Wang, Y.; Zhao, H. Exciton-exciton annihilation in $MoSe_2$ monolayers. *Phys. Rev. B: Condens. Matter Mater. Phys.* **2014**, *89*, 125427.
(38) Raja, A.; Chaves, A.; Yu, J.; Arefe, G.; Hill, H. M.; Rigosi, A. F.; Berkelbach, T. C.; Nagler, P.; Schller, C.; Korn, T.; Nuckolls, C.; Hone, J.; Brus, L. E.; Heinz, T. F.; Reichman, D. R.; Chernikov, A. Coulomb engineering of the bandgap and excitons in two-dimensional materials. *Nat. Commun.* **2017**, *8*, 15251.
(39) Yuan, L.; Chung, T.-F.; Kuc, A.; Wan, Y.; Xu, Y.; Chen, Y. P.; Heine, T.; Huang, L. Photocarrier generation from interlayer charge-transfer transitions in WS2-graphene heterostructures. *Science Advances* **2018**, *4*, No. e1700324.
(40) Brosseau, C. *Fundamentals of Polarized Light: A Statistical Optics Approach*; Wiley-Interscience, 1998.
(41) Le Roy-Brehonnet, F.; Le Jeune, B. Utilization of Mueller matrix formalism to obtain optical targets depolarization and polarization properties. *Prog. Quantum Electron.* **1997**, *21*, 109−151.
(42) Yoo, S.; Park, Q.-H. Polarimetric microscopy for optical control and high precision measurement of valley polarization. *Rev. Sci. Instrum.* **2018**, *89*, 063118.
(43) Berkdemir, A.; Gutirrez, H. R.; Botello-Mndez, A. R.; Perea-López, N.; Elías, A. L.; Chia, C.-I.; Wang, B.; Crespi, V. H.; Lpez-Uras, F.; Charlier, J.-C.; Terrones, H.; Terrones, M. Identification of individual and few layers of WS_2 using Raman Spectroscopy. *Sci. Rep.* **2013**, *3*, 1755.
(44) Kioseoglou, G.; Hanbicki, A. T.; Currie, M.; Friedman, A. L.; Jonker, B. T. Optical polarization and intervalley scattering in single layers of MoS_2 and $MoSe_2$. *Sci. Rep.* **2016**, *6*, 25041.
(45) Poellmann, C.; Steinleitner, P.; Leierseder, U.; Nagler, P.; Plechinger, G.; Porer, M.; Bratschitsch, R.; Schller, C.; Korn, T.; Huber, R. Resonant internal quantum transitions and femtosecond radiative decay of excitons in monolayer WSe_2. *Nat. Mater.***2015**, *14*, 889−893.
(46) Maialle, M. Z.; de Andrada e Silva, E. A.; Sham, L. J. Exciton spin dynamics in quantum wells. *Phys. Rev. B: Condens. Matter Mater. Phys.* **1993**, *47*, 15776−15788.
(47) Zhang, Y. J.; Oka, T.; Suzuki, R.; Ye, J. T.; Iwasa, Y. Electrically Switchable Chiral Light-Emitting Transistor. *Science* **2014**, *344*, 725−728.
(48) Ruppert, C.; Aslan, O. B.; Heinz, T. F. Optical Properties and Band Gap of Single- and Few-Layer $MoTe_2$Crystals. *Nano Lett.* **2014**, *14*, 6231−6236.
(49) Froehlicher, G.; Lorchat, E.; Berciaud, S. Direct versus indirect band gap emission and exciton-exciton annihilation in atomically thin molybdenum ditelluride ($MoTe_2$). *Phys. Rev. B: Condens. Matter Mater. Phys.* **2016**, *94*, 085429.
(50) Robert, C.; Picard, R.; Lagarde, D.; Wang, G.; Echeverry, J. P.; Cadiz, F.; Renucci, P.; Högele, A.; Amand, T.; Marie, X.; Gerber, I. C.; Urbaszek, B. Excitonic properties of semiconducting monolayer and bilayer $MoTe_2$. *Phys. Rev. B: Condens. Matter Mater. Phys.* **2016**, *94*, 155425.
(51) Neumann, A.; Lindlau, J.; Colombier, L.; Nutz, M.; Najmaei, S.; Lou, J.; Mohite, A. D.; Yamaguchi, H.; Högele, A. Opto-valleytronic imaging of atomically thin semiconductors. *Nat. Nanotechnol.* **2017**, *12*, 329−334.
(52) Zhu, B.; Zeng, H.; Dai, J.; Gong, Z.; Cui, X. Anomalously robust valley polarization and valley coherence in bilayer WS_2. *Proc. Natl. Acad. Sci. U. S. A.* **2014**, *111*, 11606−11611.
(53) Liu, Q.; Zhang, X.; Zunger, A. Intrinsic Circular Polarization in Centrosymmetric Stacks of Transition-Metal Dichalcogenide Compounds. *Phys. Rev. Lett.* **2015**, *114*, 087402.
(54) Suzuki, R.; Sakano, M.; Zhang, Y.; Akashi, R.; Morikawa, D.; Harasawa, A.; Yaji, K.; Kuroda, K.; Miyamoto, K.; Okuda, T.; Ishizaka, K.; Arita, R.; Iwasa, Y. Valley-dependent spin polarization in bulk MoS 2 with broken inversion symmetry. *Nat. Nanotechnol.* **2014**, *9*, 611.
(55) Seyler, K. L.; Zhong, D.; Klein, D. R.; Gao, S.; Zhang, X.; Huang, B.; Navarro-Moratalla, E.; Yang, L.; Cobden, D. H.; McGuire, M. A.; Yao, W.; Xiao, D.; Jarillo-Herrero, P.; Xu, X. Ligand-field helical luminescence in a 2D ferromagnetic insulator. *Nat. Phys.* **2018**, *14*, 277.
(56) Zhong, D.; Seyler, K. L.; Linpeng, X.; Cheng, R.; Sivadas, N.; Huang, B.; Schmidgall, E.; Taniguchi, T.; Watanabe, K.; McGuire, M. A.; Yao, W.; Xiao, D.; Fu, K.-M. C.; Xu, X. Van der Waals engineering of ferromagnetic semiconductor heterostructures for spin and valleytronics. *Science Advances* **2017**, *3*, No. e1603113.

DOI: 10.1021/acsphotonics.8b01306
ACS Photonics XXXX, XXX, XXX−XXX